J. Wind Eng. Ind. Aerodyn. 116 (2013) 21–31

Contents lists available at SciVerse ScienceDirect

Journal of Wind Engineering and Industrial Aerodynamics

journal homepage: www.elsevier.com/locate/jweia

Small-scale wind energy portable turbine (SWEPT)

Ravi Anant Kishore, Thibaud Coudron, Shashank Priya *

Center for Energy Harvesting Materials and Systems (CEHMS), Bio-Inspired Materials and Devices Laboratory (BMDL), Center for Intelligent Material Systems and Structures (CIMSS), Virginia Tech, Blacksburg, VA 24061, United States

ARTICLE INFO

Article history:
Received 11 July 2012
Received in revised form
4 January 2013
Accepted 16 January 2013
Available online 19 March 2013

Keywords:
Small scale wind turbine
Diffuser augmented wind turbine
Computational Fluid Dynamics
Portable power
Wind energy

ABSTRACT

This paper reports the design and characterization of a small-scale wind energy portable turbine (SWEPT) targeted to operate below 5 m/s wind speed. Aerodynamic performance characteristics of SWEPT were extensively examined using the wind tunnel experimentation and it was found that the maximum coefficient of performance of 14% occurred at the tip speed ratio of 2.9. SWEPT was found to have very low cut-in wind speed of 2.7 m/s and it produced 0.83 W of electrical power at the rated wind speed of 5 m/s. Further, we designed a diffuser structure for SWEPT using Computational Fluid Dynamics (CFD) simulations. It was observed that the SWEPT having diffuser of almost same length as the diameter of SWEPT can produce 1.4 to 1.6 times higher electrical power. An alternative method for the mechanical power calculation is also discussed which does not require torque measurement device and thus is highly useful for common laboratory measurements.

1. Introduction

Wind energy is one the most widely used renewable energy resources. However, the majority of research done till date has been mainly concentrated towards mid-to-large scale wind turbines. The recent development in the field of power electronics have reduced the power consumption of electronic devices several fold which makes viable to develop wind power applications such as structural health monitoring sensor nodes on bridges and highways, security systems in common household, and carry-on modular windmills. Unfortunately, the design models and the optimal operating conditions proposed for the large-scale wind turbines do not directly apply towards the small scale wind turbines. The small-scale wind turbines have quite different aerodynamic behavior than their large-scale counterparts. The aerodynamic behaviors of a wind turbine are primarily influenced by Reynolds number of the airfoil used for the turbine blades. Reynolds number of an airfoil is given by

$$Re = \frac{\rho c v}{\mu} \tag{1}$$

where ρ and μ are density and dynamic viscosity of the flowing fluid respectively, c denotes the chord length of the airfoil and v is the wind speed. Reynolds number is proportional to the chord length and the wind speed. For the small scale wind turbines, these two factors have very small value and therefore they operate at much lower Reynolds number as compared to the large scale wind turbines. Fig. 1 shows the effect of Reynolds number on the lift and drag coefficients for NACA 0012 airfoil (Musial and Cromack, 1988). It is very interesting to note that the maximum lift coefficient decreases with decrease in Reynolds number while the drag coefficient increases when Reynolds number is reduced. This implies that the lift to drag ratio reduces sharply with decrease in Reynolds number, which results in poor performance of the small scale wind turbines. There are myriad kinds of airfoil available these days which have been developed for different purposes. Each of these airfoils has specific range of flow Reynolds number where it performs efficiently. Selection of an appropriate airfoil, which is suitable for the operating range of a given Reynolds number, is the first and foremost step for achieving acceptable performance of a small scale wind turbine.

The power P extracted by the wind turbine is given as

$$P = \frac{1}{2}\eta\rho\pi r^2 u_\infty^3 \tag{2}$$

where r is the radius of the wind turbine, u_∞ is the speed of the wind and η is the overall efficiency of the system whose maximum value is equal to 16/27 (called the Betz's limit). The power output is proportional to the square of the radius of wind turbine and cube of the wind velocity. As the size of the wind turbine and the wind speed decrease, the power decreases drastically and below certain limit its magnitude is too low to justify the construction and operational cost. Power output is not the only important consideration in the design of small wind turbines rather other structural factors such as modularity, reliability, and cost-effectiveness have to be taken into account.

* Corresponding author. Tel.: +1 540 231 0745; fax: +1 540 231 2903.
E-mail address: spriya@vt.edu (S. Priya).

0167-6105/$ - see front matter © 2013 Elsevier Ltd. All rights reserved.
http://dx.doi.org/10.1016/j.jweia.2013.01.010

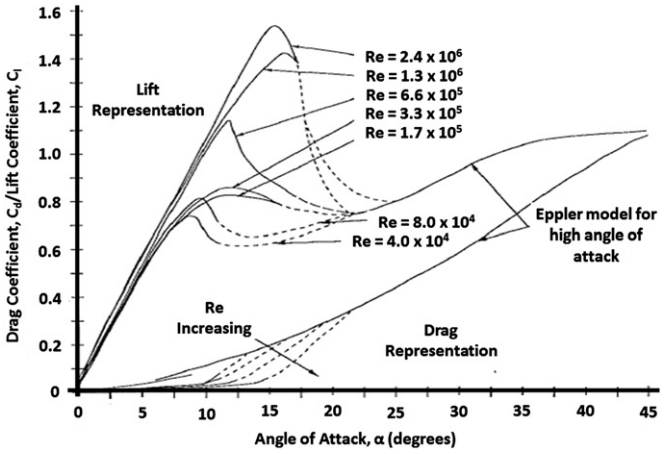

Fig. 1. Influence of Reynolds number on airfoil (NACA-0012) behavior (Musial and Cromack, 1988).

An important metric while working on the small scale is the cut-in speed. This represents the undisturbed upstream speed of the wind at which the turbine starts producing power. It depends on the total inertia and the internal friction of the system including the rotor, ball bearings, gear train and generator. The smaller the wind turbine the lower is cut-in speed due to lower inertia but the problem lies in the fact that decrease in the size of wind turbine blades reduces the aerodynamic torque and thus increases the cut-in speed. These two opposing factors should be optimized to design a wind turbine of small size but of the desired cut-in speed and power-output. The cut-in speed and the efficiency of the wind turbine may also be improved by reducing the frictional losses from the bearings and the gear train. The gear train and bearing can be avoided if the generator is directly connected to the wind turbine. However, this presents challenge in terms of achieving desired revolutions per minute (rpm) of the rotor shaft. Therefore, selection of a small size generator with the low starting torque and high voltage-to-rpm ratio is a key step. Determining the gear ratio is another important step which needs to be done when the power transmitting gearbox is unavoidable. Gear ratio depends on the range of speed and torque needed by the generator to perform most efficiently. Sometimes, size of the nacelle also restricts size of the gear box and thus the gear ratio. Cost, noise and reliability in operation are the three main factors which should be taken into account while finalizing the type and configuration of gearing system.

Apart from the factors discussed above, there are some geometrical parameters of the wind turbine blades which are needed to be optimized. The most important ones are the twist angle, blade angle, tapering angle, chord length and number of blades. Since the small scale wind turbines need to start and operate at low wind speed, their blades should have high starting torque coefficient necessary to overcome the cogging torque of the generator. Solidity of the blades is another important feature which directly affects the power coefficient of a wind turbine. It is proportional to the chord length and the number of blades. Increase in solidity increases both lift and drag forces and thus it needs to be optimized to achieve highest possible lift to drag ratio.

In summary, the design procedure for a small scale wind turbine consists of the following major steps:

(i) Selection of an airfoil suitable for low Reynolds number applications
(ii) Optimization of geometric parameters of the turbine blades for large starting torque coefficient
(iii) Determining the optimal gear ratio of the drive train based upon the speed and torque requirement of the generator
(iv) Generator selection with high voltage-to-rpm ratio and low starting torque

There is no fixed nomenclature defined in the literature to categorize the wind turbines on the basis of their size. We define the nomenclature for the wind turbines as: (i) micro-scale (diameter < 10 cm), (ii) small-scale (10 cm $<$ diameter $<$ 100 cm), (iii) mid-scale (1 m $<$ diameter $<$ 5 m) and (iv) large-scale (diameter > 5 m). All the discussion made in this paper is based on this nomenclature.

There are very limited numbers of studies reported in literature related to the wind turbines of diameter less than 1 m designed for the wind speed below 10 m/s. Hirahara et al., (2005) studied a small scale wind turbine (named as μF500) of 50 cm diameter using NACA 2404 blade template. μF500 has four fan-type blades unlike the traditional wind turbines which usually have 2–3 tapered-type blades. This turbine performs quite efficiently with the optimal power coefficient of 0.36 and the net efficiency of 0.25 in the wind speed range of 8–10 m/s. Leung et al., (2010) presented the computational and experimental studies on the multi-bladed small scale-wind turbines. They suggested that since the blades are quite small, the small scale-wind turbines can have fan type of blades of uniform thickness along the entire span instead of the traditional airfoil and taper type blades. These fan type blades with constant chord length have higher solidity and thus provide functional advantage of increase in power efficiency. Another interesting study has been performed by Vardar and Alibas, (2008) where they compared the rotation rates and the power coefficients of the small scale-wind turbines manufactured using the different NACA profiles for the various geometrical parameters like the twist angle, blade angle and the number of blades. Out of four blade profiles (namely NACA 0012, NACA 4412, NACA 4415, and NACA 23012) tested, it was found that NACA 4412 profiles with 0 grade twisting angle, 5 grade blade angle and double blades had the highest rotation rate, while NACA 4415 profiles with 0 grade twisting angle, 18 grade blade angle, 4 blades had the highest power coefficient.

The efficiency and power output of small scale wind turbines are generally lower than that of large scale wind turbines. It has been suggested by some researchers (Abe and Ohya, 2004; Abe et al., 2005; Foreman et al., 1978; Matsushima et al., 2006; Ohya et al., 2008) that a duct in the form of diffuser can enhance the overall power output of a wind turbine. Further, it also improves the cut-in wind speed and thus allows wind turbines to operate at lower wind speed. Different kinds of diffusers have been developed over the period of time and the power augmentation up to 4–5 times has been reported with the flanged diffuser (Ohya et al., 2008). However, incorporation of diffuser makes the device quite bulky, increases the overall aerodynamic drag and requires strong mounting.

This study presents the development of a small-scale, compact, portable and cost-effective wind turbine for the house-hold applications. The wind turbine will be mounted near the ground-level where the typical wind speed is below 5 m/s. We present the characteristics and performance of the first generation prototype termed as SWEPT (Small Scale Wind Energy Portable Turbine). Using the wind-tunnel experimentations, it was found that the SWPET has very low start-up speed of 2.7 m/s and is capable of producing the electrical power up to 0.83 W at the wind speed of 5 m/s. Its maximum coefficient of performance was found to be 14% at the optimal tip speed ratio of 2.9. The overall efficiency of SWEPT's first generation prototype is quite low and needs to be improved for the next generation prototypes by using optimized blades and better generator.

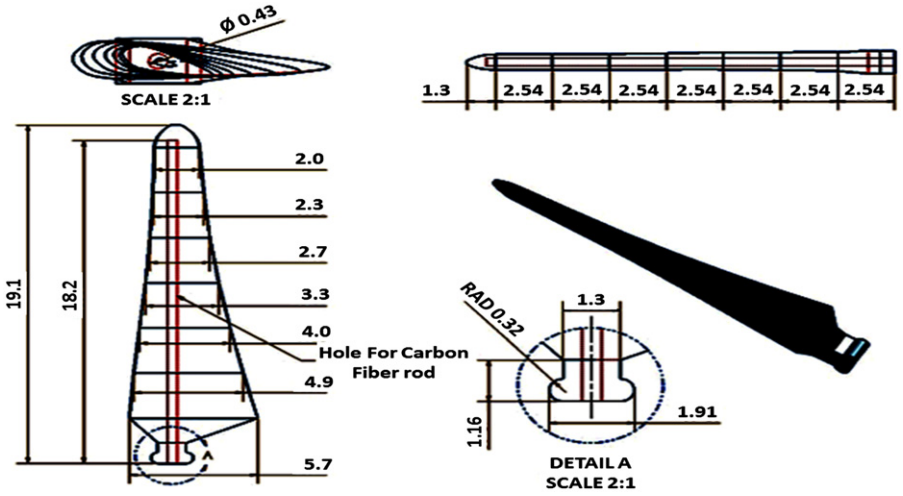

Fig. 2. SWEPT blade design configuration with all dimensions in cm.

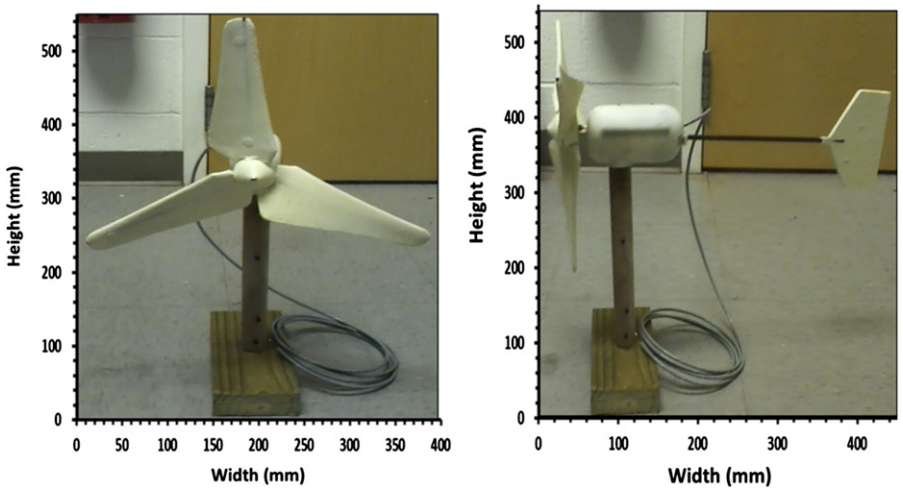

Fig. 3. First generation small-scale windmill prototype "SWEPT".

As discussed previously, the diffuser has been recently found as a potential solution to augment the power output of a wind turbine by multiple folds. To check the possibility of using diffuser for the small scale wind turbines, Computational Fluid Dynamics (CFD) studies were conducted for modeling the geometry and dimension of diffuser for SWEPT. Various geometrical parameters of the diffuser were analyzed in detail and an optimized diffuser was developed which provided maximum power amplification within given size constraints. Wind tunnel experiments were then conducted with the diffuser augmented-SWEPT and experimental results were found to be in close agreement with the CFD predictions. It was noted that the ducted-SWEPT with optimized diffuser having length approximately equal to the diameter of SWEPT produced 1.4 to 1.6 times higher power output than the normal SWEPT.

2. Swept: design specifications and construction

SWEPT is a three-blade, 39.4 cm diameter, horizontal axis, small scale wind turbine. Its blades are linearly twisted by 32° from root to tip and their connection angle to the hub is 3°. The airfoil used is symmetrical along the camber line and had maximum thickness of 6.5 mm throughout the span of the blades. Fig. 2 shows the details of the blade profile with all dimensions in centimeters. Blades are connected to the aerodynamically shaped hub using dove-tail joints. SWEPT has a gear train of gear-ratio 80:10 which are needed to amplify the rotational speed of the driving shaft of the generator. The permanent magnet direct current motor has been used as the generator as there was no suitable generator/alternator readily available of the desired size. A 24 V permanent magnet DC motor manufactured by Mabuchi Motor Co. Ltd. (model # 14415) was selected as the generator. Blades and hub of SWEPT were casted to ensure the reliability of manufacturing process and also to reduce the cost associated with fabrication. The casting material used was 'Feather Lite' low density urethane casting resin produced by Smooth-on, Inc. 'Feather Lite' has low weight-to-strength ratio so that the rotating components have low inertia but high strength. Carbon fiber rods were incorporated in the mid-plane of the blades while casting as an additional reinforcement. Fig. 3 shows a fully assembled SWEPT prototype.

3. Diffuser: design optimization and construction

Theoretically, the power output by a wind turbine is proportional to cube of the wind speed. It implies that any method, which can increase the wind speed around the turbine even by a small factor, can largely improve the power output. The diffuser

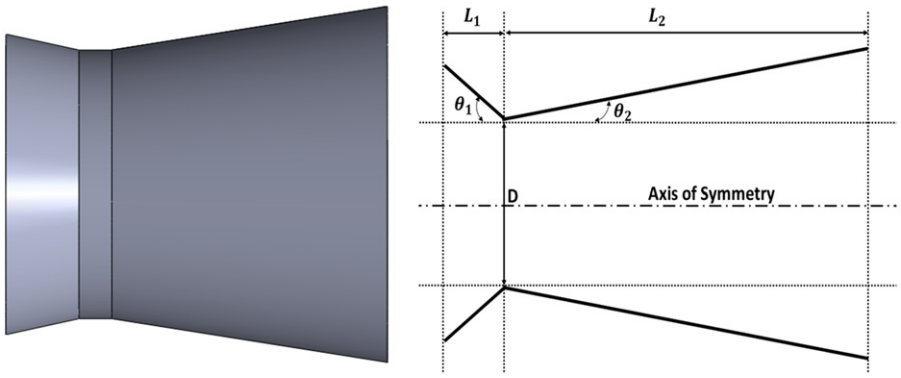

Fig. 4. An initial design of diffuser modeled using CFD.

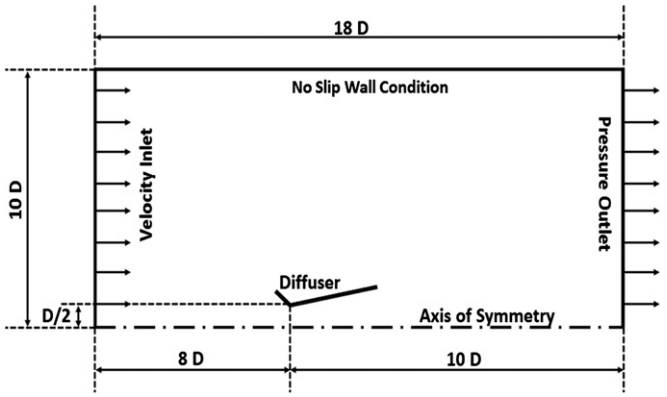

Fig. 5. Two-dimensional computational domain with boundary conditions.

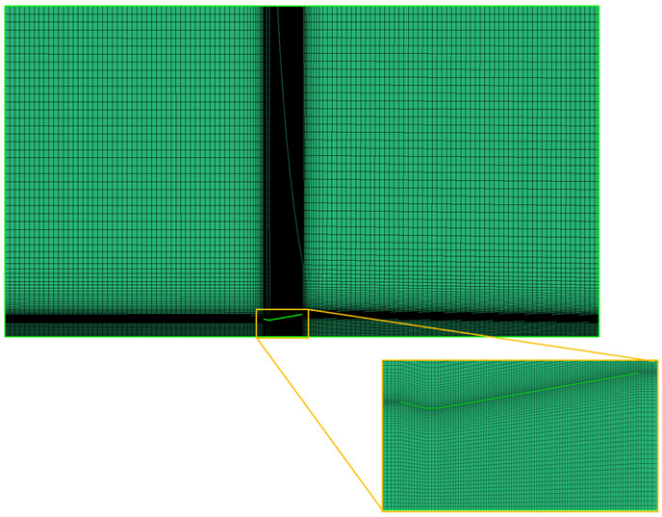

Fig. 6. Two-dimensional grid system.

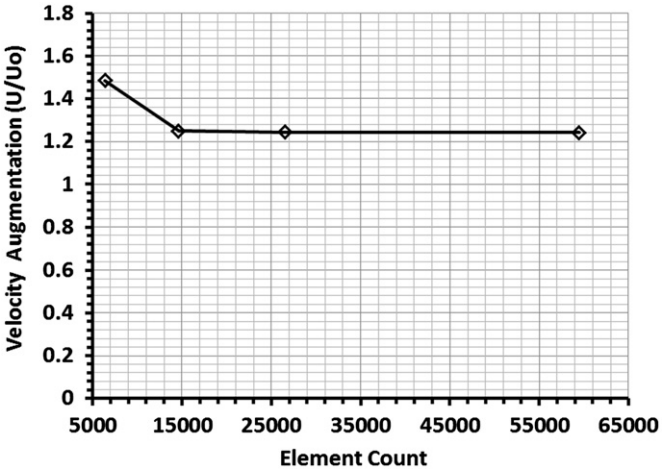

Fig. 7. Mesh independency test.

allows turbine's exhaust flow to expand and thus produces sub-atmospheric pressure in the region near to turbine exit. The low pressure region draws more wind and allows it to accelerate. This is the reason for a ducted wind turbine with a diffuser to exhibit higher power output than a wind turbine without diffuser (Foreman et al., 1978).

Considering the 3D manufacturing processes, it was decided to simplify the diffuser geometry. As shown in Fig. 4, the diffuser consisted of three parts: a converging section, a 1-in. long throat and a diverging section. There are essentially four geometrical parameters which needed to be optimized, namely (a) converging section length L_1, (b) converging section half cone angle θ_1, (c) diverging section length L_2 and (d) diverging section half cone angle θ_2. Computational Fluid Dynamics (CFD) has been used in literature (Abe and Ohya, 2004; Abe et al., 2005; Wang et al., 2008) to model the diffuser design. In this study we utilized commercial fluids package fluent (ANSYS Inc., USA) to study the flow field through and around the diffuser. The effect of each geometrical parameter on the velocity augmentation was extensively examined and an optimal geometry was derived. Wind tunnel experiment was conducted to verify the numerical results.

3.1. Solution strategy

The flow inside the diffuser is axis symmetrical, therefore, 2-dimensional model was considered to reduce the simulation time. Fig. 5 shows the computational domain of the diffuser along with the area inside a hypothetical wind tunnel. The wind tunnel has diameter 20 times that of diffuser throat diameter. Entrance and exit lengths before and after the diffuser were approximately 8 and 10 times of the diffuser throat diameter respectively. Such a large wind tunnel around the diffuser will ensure that the boundary layer effect of the walls of the tunnel does not affect the flow inside the diffuser. Also, relatively bigger fluid domain around the diffuser mitigates the effects of obstruction and blockage to the free stream (Abe and Ohya, 2004; Matsushima et al., 2006; Wang et al., 2008). Velocity-inlet and pressure outlet boundary conditions were specified at the entrance and exit of the fluid domain respectively. Turbulence intensity as 10% with

length scale as 1 m has been assumed at the velocity-inlet boundary condition. The walls of the wind tunnel and the diffuser were assigned no slip boundary condition. As mentioned later in the paper that we have used SST $k-\omega$ turbulence model, which provides 'enhanced wall treatments' to the wall boundary conditions i.e. all the boundary conditions for the coarse meshes are treated as the wall function approach, while for the fine meshes, the appropriate low-Reynolds-number boundary conditions are applied (FLUENT, 2009). Symmetry boundary condition was specified for the axis, as the system was symmetrical about it. The free stream velocity of 4.1 m/s was taken for all the numerical calculations. Fig. 6 shows the 2-dimensional grid system generated using ICEM CFD (ANSYS Inc., USA) commercial software. Total number of elements was 26500 with very fine meshing in the region inside the diffuser and relatively coarser mesh outside. The element counts inside the diffuser were about 4000 with approximately 100 nodes in axial direction and 40 nodes along radial direction. We performed mesh independency test to ensure that variation in number of elements should not affect the solution. The simulations were run at different number of elements between 6000 and 60000 and it was found that the variation in result from element count of 26,500 to 59,500 was less than 0.5%. Fig. 7 shows the effect of element count on the velocity augmentation factor U/U_o by one of the diffuser model at the wind speed of $U_o=4.1$ m/s.

The shear-stress transport (SST) $k-\omega$ model has been used as the turbulence model for all the numerical simulations in this study. The advantage of using SST $k-\omega$ over the standard turbulence models like $k-\omega$ and $k-\varepsilon$ is that it effectively blends the robustness and accurate formulation of the $k-\omega$ model in the near-wall region with the free-stream independency of the $k-\varepsilon$ model in the far field (FLUENT, 2009). It is believed that the use of SST $k-\omega$ model provides better results for the flow-field predictions with the adverse pressure gradient. The area-weighted average velocity across the cross-sectional area near the throat of the diffuser was used to calculate the velocity amplification factor. Each diffuser design parameter discussed in the previous section was varied individually by keeping other variables constant to understand its effect on the velocity augmentation.

3.2. Diffuser design optimization

Fig. 8 (a) and (b) shows the effect of converging section length L_1 and half cone angle θ_1 on the velocity amplification factor of the diffuser. The numerical simulations were conducted at four different values of converging section length L_1 varying from 0.125 D to 0.5 D and eight different values of converging section half cone angle ranging from 0^o to 21^o. At the given values of diverging section length $L_2=1.0$ D (Fig. 8(a)) and $L_2=1.5$ D (Fig. 8(b)), and half cone angle $\theta_2=10^o$, the velocity augmentation factor U/U_o increases with increase in converging section length L_1, when θ_1 is fixed. However, the effect is not so prominent and therefore the smallest value $L_1=0.125$ D has been selected considering the size constraint and to minimize the cost of material. It can also be noted in these figures that when L_1 is fixed, the velocity augmentation factor U/U_o slowly increases with increase in the value of θ_1 from 0^o to 15^o but saturates beyond this range. Fig. 9 represents the effect of diverging section length L_2 and half cone angle θ_2 at the fixed values of converging section length $L_1=0.125$ D and half cone angle $\theta_1=15^o$. It can be seen that the velocity augmentation factor U/U_oincreases continuously with increases in the value of θ_2 from 0^o to 16^o when $L_2=0.5$ D. However, when $L_2=1.0$ D and 1.5 D, factor U/U_ohas a

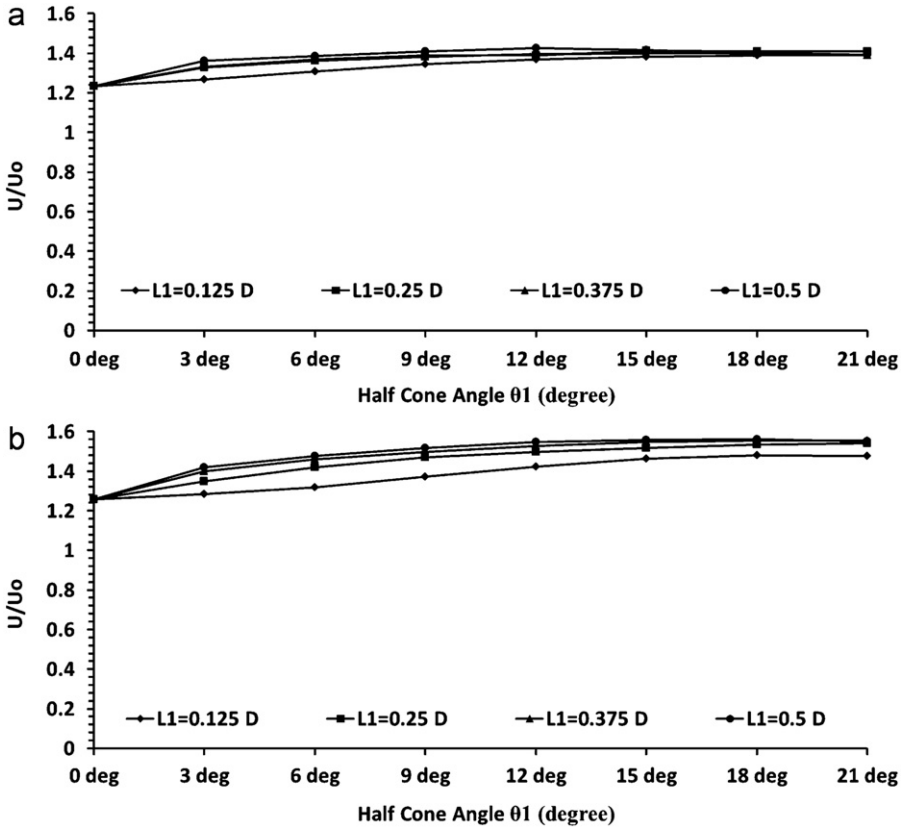

Fig. 8. (a). Effect of converging section length L_1 and half cone angle θ_1 on velocity augmentation factor U/U_o ($L_2=1.0$ D and $\theta_2=10^o$), (b). Effect of converging section length L_1 and half cone angle θ_1 on velocity augmentation factor U/U_o ($L_2=1.5$ D and $\theta_2=10^o$).

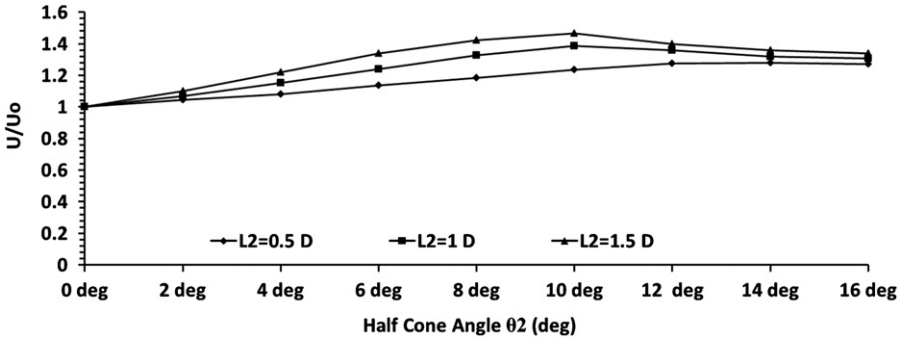

Fig. 9. Effect of diverging section length L_2 and half cone angle θ_2 on velocity augmentation factor U/U_o (L_1=0.125 D and half cone angle θ_1=15°).

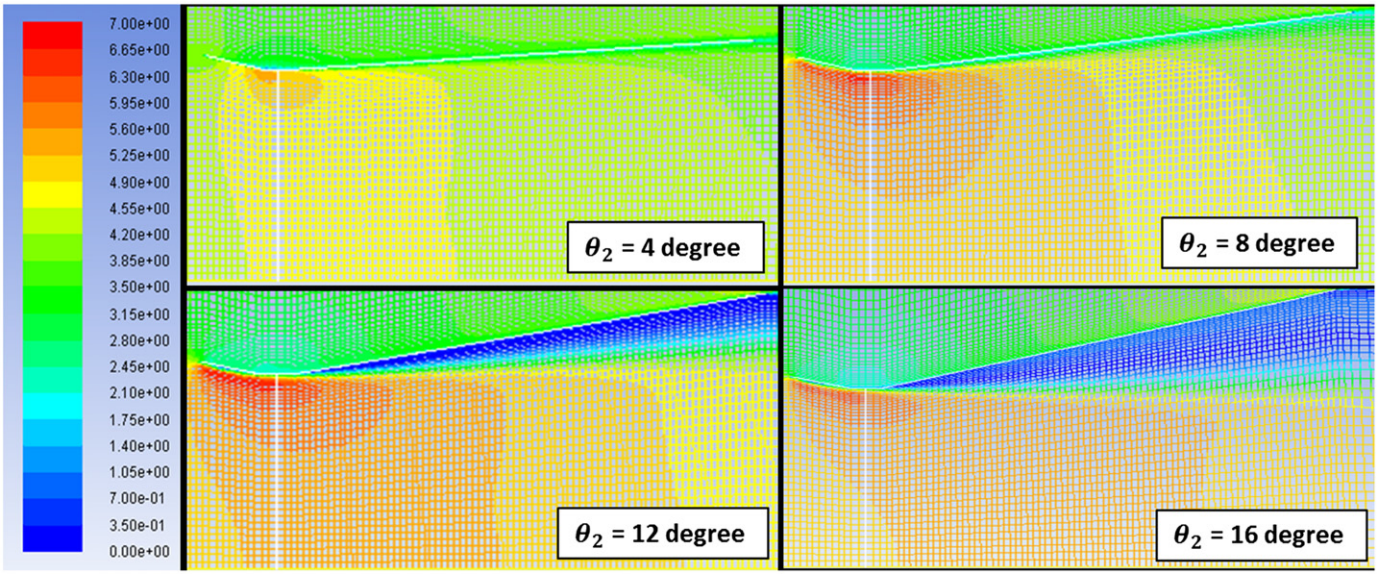

Fig. 10. Velocity contours at different θ_2 (L_2=1.0 D, L_1=0.125 D, θ_1=15°).

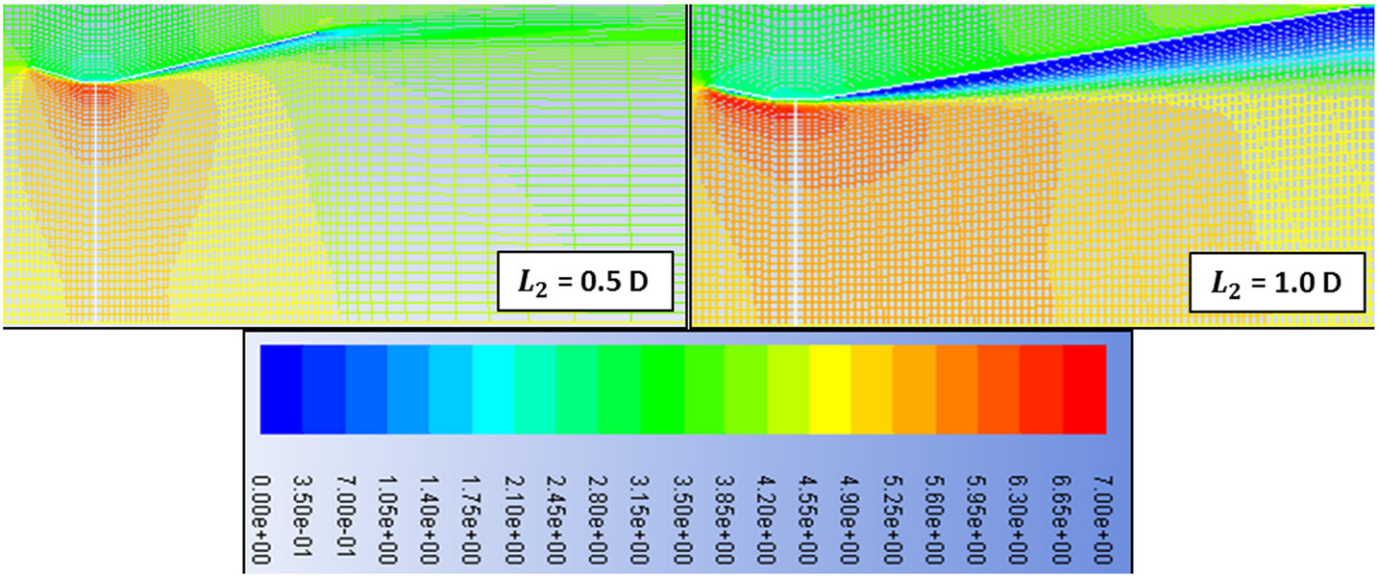

Fig. 11. Velocity contours at different L_2 (θ_2=12°, L_1=0.125 D, θ_1=15°).

maxima at θ_2=10°. Also, U/U_o increases continuously with increase in the value of L_2 when other variables are fixed.

It can be concluded from this analysis that the diverging section has very strong effect on the velocity augmentation by the diffuser. Higher value of expansion angle θ_2 allows flow-field to expand. However, flow tends to separate from the wall of diffuser when expansion angle is too large. Separation of the flow is generally not desirable because it deteriorates the performance

of the device. The attachment and detachment of the flow are not only controlled by the expansion angle but also by the length of the diverging section. Flow may remain attached even at larger expansion angle, if length of the diverging section is smaller. Fig. 10 and 11 show the velocity contours obtained during post-processing of CFD results. Violet region near the wall of the diffuser in some of the contours shows flow separation. All the contours of Fig. 10 have been obtained for $L_1=0.125$ D, $\theta_1=15^o$ and $L_2=1.0$ D at the wind speed of 4.1 m/s. It can be seen that flow is attached when $\theta_2=4^o$ and $\theta_2=8^o$, it detaches at $\theta_2=12^o$ and separation region is much bigger at $\theta_2=16^o$. This explains the reason as to why velocity augmentation factor U/U_o is maximum at $\theta_2=10^o$ when $L_2=1.0$ D in Fig. 9. Contours of Fig. 11 show the effect of diverging section length on flow separation. At $\theta_2=12^o$, flow separates when $L_2=1.0$ D but it is still attached to the wall of diffuser when $L_2=0.5$ D. The consequence of this effect is clear in Fig. 9, velocity augmentation factor U/U_o decreases when $\theta_2 \geq 12^o$ at $L_2=1.0$ D but it continues to increase for the case $L_2=0.5$ D. As stated above, the effect of converging section on the velocity augmentation is not so strong, but it makes the flow more concentrated before it starts to expand in diverging section. Table 1 summaries the range of various variables studied and their optimal value selected on the basis of velocity augmentation factor U/U_o and size constraint of the diffuser.

3.3. Diffuser construction

The main challenge before constructing the diffuser was to make it as light in weight as possible while keeping the manufacturing process compatible with 3D molding and casting. The diffuser construction was completed in two steps. First, a prototype was constructed using metallic sheet and then this prototype was used as mold to make actual diffuser using fiber reinforced plastics by hand lay-up process. The composite consists of three layers of fibers: one layer of glass fiber sandwiched between two layers of carbon fiber with epoxy resin as the bonding agent. Fig. 12 shows the diffuser mold constructed from metal sheet and the final product made up of carbon and glass fiber reinforced plastics.

Table 1
Diffuser design parameters.

Parameters	Symbol	Range	Optimal value
Converging section length	L_1	0.125–0.5 D	0.125 D
Converging section half cone angle	θ_1	0°–21°	15°
Diverging section length	L_2	0.5–1.5 D	1.0 D
Diverging section half cone angle	θ_2	0°–16°	10°

3.4. Experimental verification

Wind tunnel experiment was conducted on diffuser without turbine inside to know the actual velocity augmentation. The details of the experimental set-up and wind tunnel experiment will be discussed in the next section. In this section, we will compare the numerical data on the velocity augmentation factor with the experimental performance. Fig. 13 depicts the velocity augmentation factor at the center of the throat of the diffuser found experimentally and calculated numerically. It can be seen that the velocity augmentation factor U/U_o is almost constant with the wind speed. Numerical results are, however, slightly higher than the experimental data. One of the reasons for this difference in numerical and experimental results can be related to the blockage effect. While in computational modeling, we purposely defined much larger fluid domain around the diffuser in order to avoid blockage to the flow, however, during experimentation, we did not have availability of such wind tunnel with large cross-sectional area. Next, the wind tunnel experiment was re-conducted to know the performance and power augmentation factor of ducted-SWEPT over normal SWEPT at various wind speeds. These results will be described in Results and Discussion section.

4. Experimental set-up

All the experiments were conducted using the Subsonic Open Jet Wind Tunnel facility available at Virginia Tech. This is 0.7 m long, blower type, open circuit wind tunnel which is known for its high quality flow. It is powered by a 30 hp BC-SW size 365 Twin

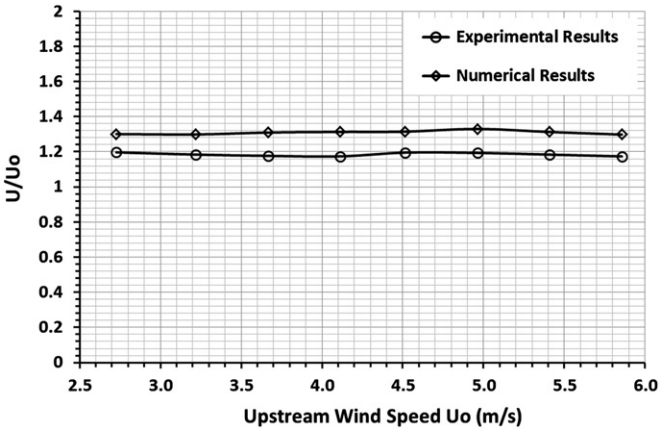

Fig. 13. Comparison of velocity augmentation factor obtained numerically and experimentally.

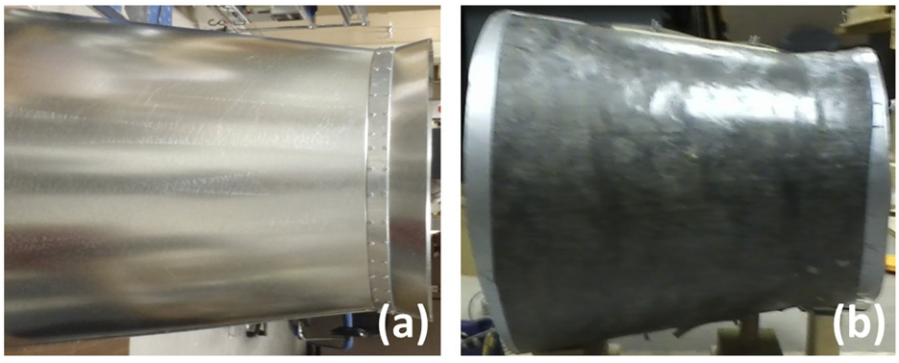

Fig. 12. Diffuser made up of (a) metal sheet and (b) fiber reinforced plastics.

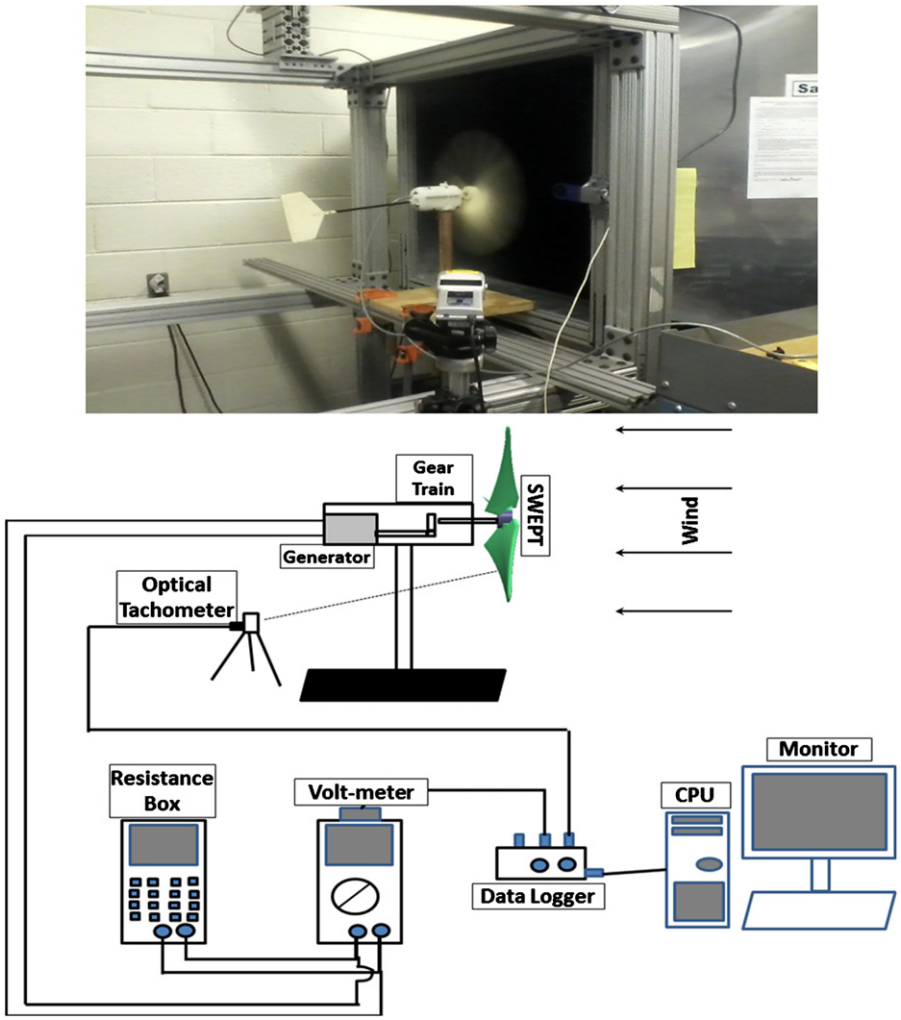

Fig. 14. Experimental set-up with the schematic diagram.

City centrifugal fan. The air flow discharged by the fan first passes through a 6°-4 m long diffuser, which is then directed into a $1.47 \times 1.78\ m^2$ settling chamber followed by a combination of 0.01 m cell size, 0.09 m long honeycomb and three turbulence reduction screens which ensure a uniform flow with low turbulence, less than 2%. The flow is finally discharged in the atmosphere through a 5.5:1 contraction nozzle based on a 5th degree polynomial profile. The maximum obtainable wind speed of the wind tunnel is 28 m/s. The wind tunnel is also equipped with a jet catcher, which is located 1.2 m downstream of the contraction exit, to minimize the impact of the flow on the lab environment.

The angular velocity of the wind turbine was measured using non-contact type optical, digital Tachometer 'DT-209X' (SHIMPO Instruments, USA). Anemometer used in the experiments was PASPORT, Model PS-2174 (PASCO, USA). The output voltage of the wind turbine generator was measured using 'RadioShack Digital Multi-meter'. The resistance box used to study the performance of the wind turbine at various loading conditions was an electronically controlled resistance box named 'ohmSOURCE Model OS-260' by IET Labs, Inc. Fig. 14 shows the experimental set-up and schematic diagram of the wind tunnel experimentation. The generator of the wind turbine was connected to the voltmeter which was connected to the resistance box in parallel. At a fixed wind velocity, the load resistance can be varied using the resistance box and corresponding output voltage can be recorded. The experiment was repeated several times for a given set of conditions and arithmetic mean of the voltage and the angular velocity recorded was taken as the representative value. We conducted the wind tunnel experiments at 8 different wind speed conditions between 1.8 m/s and 5.0 m/s. The method for mechanical power calculation is explained in the next section.

5. Results and discussion

5.1. Mechanical power by SWEPT

The mechanical power is defined as the product of torque and angular speed and it can be easily calculated for a wind turbine if we can accurately determine the torque and rpm of the rotor when wind turbine is running without any external load. Torque transducer, which is generally used to measure the shaft torque, is quite expensive device therefore an alternative method was developed in this study. This method is based on the basic relationship which defines torque as:

$$\Gamma = J\frac{d\omega}{dt} \tag{3}$$

where Γ is the torque generated by the wind turbine, J is the moment of inertia of the rotor (including blades) about the axis of rotation and $d\omega/dt$ is the time rate of change of angular speed called angular acceleration. The moment of inertia was

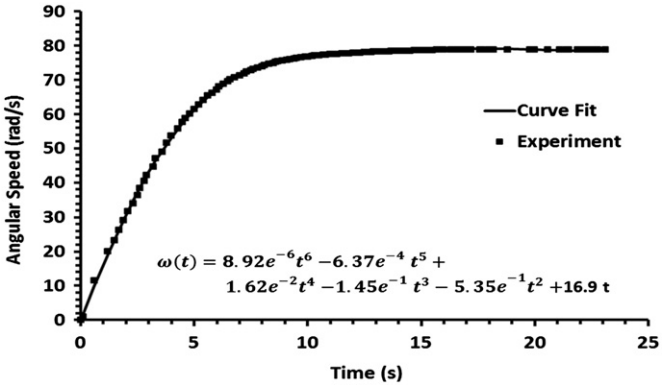

Fig. 15. Angular speed at the wind speed of 3.2 m/s.

determined using the commercial software SolidWorks. The angular acceleration was calculated using the wind tunnel experimentation. The blade of the wind turbine was held stationary until wind speed in the wind tunnel was stabilized and then it was allowed to rotate and accelerate freely to its maximum constant speed. The rpm of the turbine blade, while it was accelerating, was recorded at the time interval of 100 ms using the optical tachometer. The curve fitting method was then employed to find the 6th degree polynomial equation which describes the rpm as function of time. Fig. 15 shows the angular speed of the wind turbine at the wind speed of 3.2 m/s. The time derivative of the velocity gives the acceleration which multiplied by the moment of inertia provides the torque. Fig. 16 shows the variation of torque and the angular speed as a function of time at four different wind speeds. Torque is highest when the wind turbine is stationary and it slowly decreases to zero as the wind turbine speeds up to its maximum rpm. The mechanical power is zero at $t=0$ because rpm is zero. It reaches maximum at time interval where the torque curve and rpm curve intersect and then again decreases to zero because torque is zero. The intersection point moves up and leftward as wind speed is increased which implies that not only the magnitude of the maximum mechanical power is higher but also the response of the wind turbine is better. The angular speed at which a wind turbine generates the maximum power is called its optimal rpm. The mechanical power as a function of angular speed is shown in Fig. 17. It is interesting to note that even though the optimal rpm increases with increase in the wind speed but it is always near about 60% of the maximum rpm. The best possible overall output power from a wind turbine cannot be achieved unless and until the rated rpm of the generator is well synchronized with the turbine's optimal rpm.

5.2. Tip-Speed Ratio and Coefficient of Performance

Tip speed ratio (TSR) is the most commonly and conveniently used scaling parameter, defined as

$$\mathrm{TSR} = \frac{R\omega}{U_\infty} \tag{4}$$

where R is radius of the tip of the blade, ω is the angular speed of the rotor and U_∞ is the free wind speed. TSR is essentially used to integrate the principle aerodynamic effect of the wind speed, rotor size and rotor's angular speed with the power coefficient of the rotor (Spera, 1994). The power coefficient or coefficient of performance (Cp) of the rotor is defined as

$$\mathrm{Cp} = \frac{P}{(1/2)\rho A U_\infty^3} \tag{5}$$

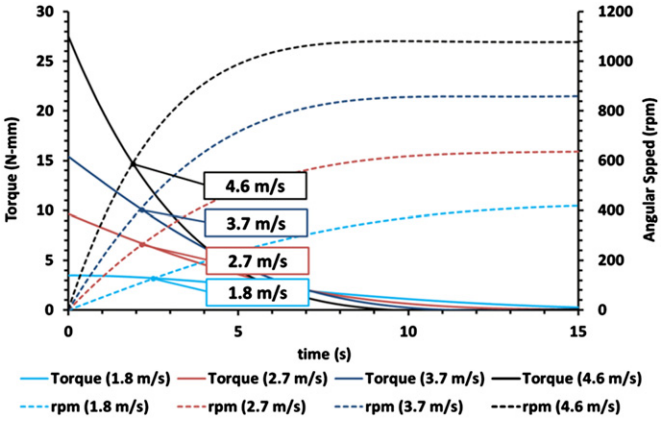

Fig. 16. Torque and rpm relationship.

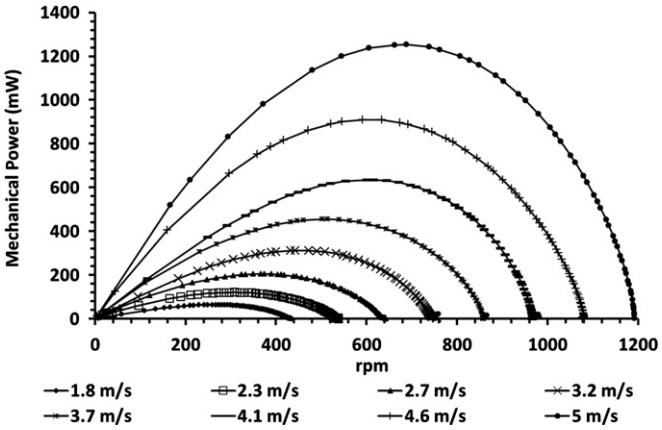

Fig. 17. Mechanical power of SWEPT at different wind speed.

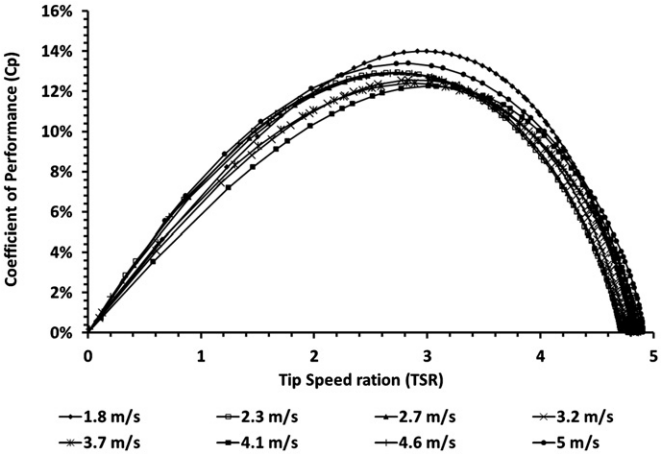

Fig. 18. Coefficient of performance vs. Tip-Speed ratio.

where P is the mechanical power generated by the wind turbine, ρ is the density of the wind, A is the swept area by the rotor and U_∞ is the free wind speed. The coefficient of performance as a function of the tip speed ratio (shown in Fig. 18) depicts the response of the wind turbine under various operating conditions. It can be observed in Fig. 18 that the coefficient of performance initially increases with the increase in the value of TSR, reaches maxima, and then decreases. This can be explained by noticing that when TSR is small it corresponds to the situation when the wind turbine is rotating very slowly and almost all wind

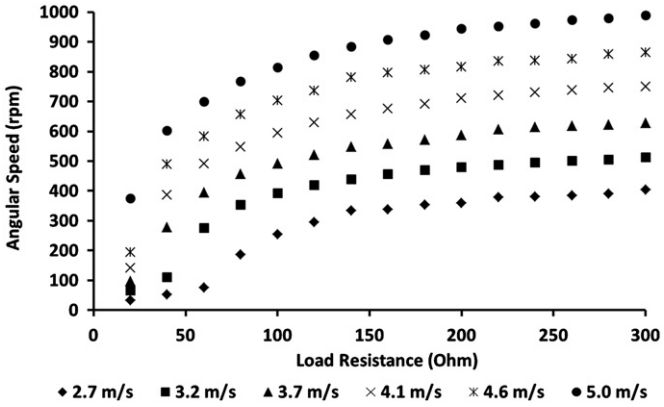

Fig. 19. Angular speed as a function of load resistance.

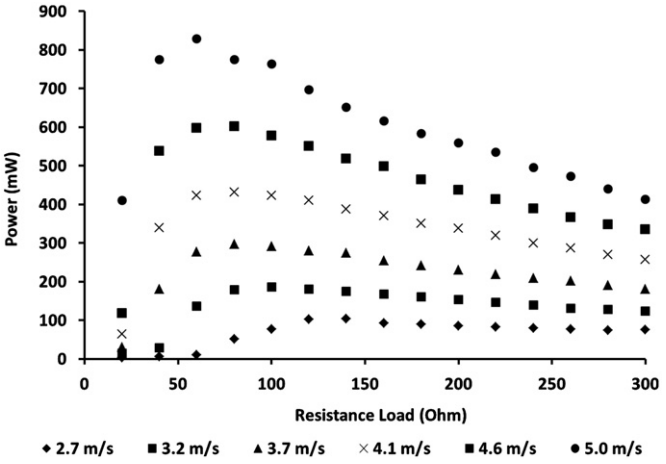

Fig. 20. Electrical power of SWEPT at different load and wind speed.

just passes across the blades without much power transfer. On the other hand, when TSR value is too large, the fast moving blades appear like a solid disc and thus the coefficient of performance decreases. Thus, tip speed ratio directly affects the power generation and therefore it is very crucial to assess the optimal TSR while designing the turbine blades (Yurdusev et al., 2006). The tip speed ratio of the large scale wind turbines is normally between 7 and 10, however for the small-scale wind turbines, low TSR in the range of 2 to 4 has been suggested for achieving reliability and noiseless driving (Hirahara et al., 2005). The maximum value of the power coefficient of SWEPT was around 14% at the tip-speed ratio of 2.9 which is well within the desirable limits.

5.3. Overall performance of SWEPT

The overall performance of a small-scale wind turbine is dependent upon all its components. Fig. 19 shows the rpm of the turbine blades under different loading conditions at six different wind speeds. It can be seen that SWEPT starts at very low wind speed of 2.7 m/s. It runs between 300 rpm and 800 rpm under the normal loading condition. The gear train has gear ratio of 80:10 and it thus allows the generator rotor to run in the range of 2400 to 6400 rpm which is reasonable speed for a motor working as a generator to produce good output voltage. At a fixed wind speed, initially the rpm of the wind turbine increases with the increase in the load resistance and it saturates after some point when load resistance is too large. This characteristic of the wind turbine arises due to a typical behavior, called motor reaction, of an electric generator. Basically, when load is applied to a running generator, it delivers current which creates a magnetic force that opposes the rotation of the armature. The strength of the reacting magnetic force depends on the armature current which is ultimately determined by the magnitude of the load resistance. Decrease in the resistive load increases the armature current and thus increases the motor reaction which eventually slows down the speed of the rotor. However, at the given loading condition, the angular speed increases with the increase in the wind speed. Higher wind speed causes larger aerodynamic torque on the turbine blades which increases the rotor's rpm, provided the wind speed is below stall limit. Fig. 20 shows the electrical behavior of SWEPT at different loading conditions. The optimal load lies between 60 Ω and 120 Ω and it decreases as the wind speed increases. The maximum power output was found to be 830 mW at the optimal load of 60 Ω for the wind speed of 5 m/s.

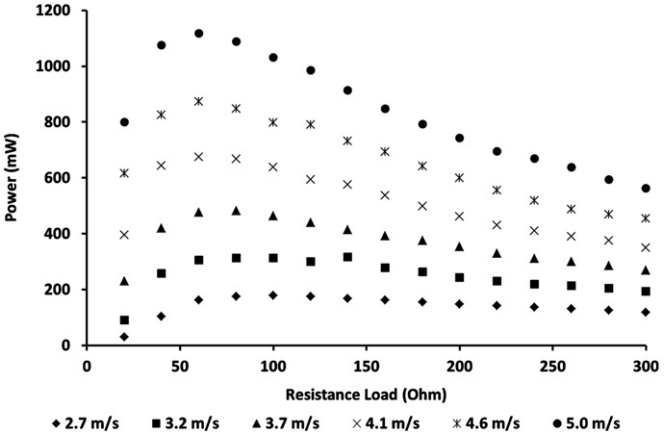

Fig. 21. Power output of diffuser augmented SWEPT at different load and wind speed.

5.4. Power generated by ducted- SWEPT

As explained earlier, a diffuser is essentially a wind acceleration system which, by virtue of its shape, creates sub-atmospheric pressure near exit and thus induces greater mass flow rate through the turbine. Fig. 13 shows that the optimized diffuser has velocity augmentation factor of about 1.2. Theoretically, power output of a horizontal axis wind turbine is proportional to the cube of upstream wind speed, which entails that the power output of ducted SWEPT should be around 1.7 times higher than the power generated by SWEPT without a diffuser. Fig. 21 shows the power output of the ducted SWEPT at various wind speeds and load resistances. The optimal power output of SWEPT with and without diffuser at various wind speeds has been compared in Fig. 22. It can be noted that the power augmentation factor P/P_o is in the range of 1.4–1.6, which is lower than the expected value of 1.7. The main reason for the lower than expected performance of diffuser is the wind turbine itself. The presence of wind turbine in the diffuser exerts resistance to the wind flow and thus it creates loading effect. The loading factor C_t of a wind turbine depends on many variables such as geometric parameters (like rotor diameter, blade twist angle, chord length and number of blades), aerodynamic properties (like lift and drag coefficients) and operating conditions (like wind speed and rpm of the rotor). Abe and Ohya, (2004) determined the value of C_t using disk loading method and showed that the acceleration factor U/U_o

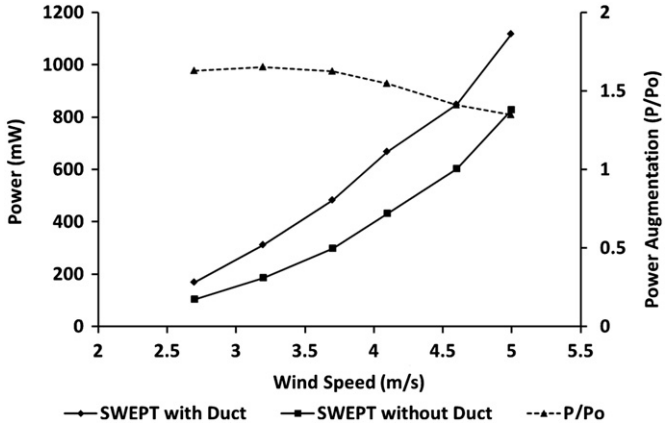

Fig. 22. Power augmentation of SWEPT with diffuser over SWEPT without diffuser.

decreases with increase in value of C_t. Besides loading, there are some other factors, mainly the aerodynamic losses associated with nacelle drag, hub/tip losses and blockage to flow because of diffuser, which can be the reason for the poorer performance of the ducted SWEPT at higher wind speed.

6. Conclusion

This paper reports the development of a small-scale wind energy portable turbine (SWEPT) which operates at wind speeds below 5 m/s. The major outcomes of the study can be summarized as below.

(1) Wind tunnel experiment shows that SWEPT has maximum coefficient of performance of 14% at the optimal tip speed ratio of 2.9.
(2) SWEPT has very low cut-in wind speed of 2.7 m/s and it is found to generate mechanical power of 1.25 W and electrical power of up to 0.83 W at the wind speed of 5 m/s.
(3) A diffuser was also designed and fabricated to contemplate its utility for the small-scale wind turbines. CFD studies revealed that the diverging section of the diffuser is stronger parameter than its converging section which influences its performance.
(4) The optimal diffuser design has converging section length of 0.125 times throat diameter and half cone angle of 15° while the length of diverging section is equal to the throat diameter with half cone angle of 10°. It produces velocity augmentation of about 1.2 times the upstream wind speed.
(5) It was observed that the diffuser-augmented SWEPT of length approximately the same as the turbine's diameter could produce 1.4–1.6 times higher power output than a SWEPT without diffuser.

Acknowledgment

The authors gratefully acknowledge the financial support provided by NIST program and NSF I/UCRC: Center for Energy Harvesting Materials and Systems (CEHMS).

References

Abe, K.-i., Ohya, Y., 2004. An investigation of flow fields around flanged diffusers using CFD. Journal of Wind Engineering and Industrial Aerodynamics 92, 315–330.
Abe, K., Nishida, M., Sakurai, A., Ohya, Y., Kihara, H., Wada, E., Sato, K., 2005. Experimental and numerical investigations of flow fields behind a small wind turbine with a flanged diffuser. Journal of Wind Engineering and Industrial Aerodynamics 93, 951–970.
FLUENT, A., 2009. Theory Guide. ANSYS FLUENT 12.0.
Foreman, K.M., Gilbert, B., Oman, R.A., 1978. Diffuser augmentation of wind turbines. Solar Energy 20, 305–311.
Hirahara, H., Hossain, M.Z., Kawahashi, M., Nonomura, Y., 2005. Testing basic performance of a very small wind turbine designed for multi-purposes. Renewable Energy 30, 1279–1297.
Leung, D.Y.C., Deng, Y., Leung, M.K.H., 2010. Design optimization of a cost-effective micro wind turbine, Proceedings of the World Congress on Engineering. WCE 2010, London, U.K.
Matsushima, T., Takagi, S., Muroyama, S., 2006. Characteristics of a highly efficient propeller type small wind turbine with a diffuser. Renewable Energy 31, 1343–1354.
Musial, W.D., Cromack, D.E., 1988. Influence of Reynolds number on performance modeling of horizontal axis wind rotors. Journal of Solar Energy Engineering (United States) 110 (2), 139–144, Medium: X.
Ohya, Y., Karasudani, T., Sakurai, A., Abe, K.-i., Inoue, M., 2008. Development of a shrouded wind turbine with a flanged diffuser. Journal of Wind Engineering and Industrial Aerodynamics 96, 524–539.
Spera, D.A., 1994. Wind turbine technology: fundamental concepts of wind turbine engineering. ASME Press, New York.
Vardar, A., Alibas, I., 2008. Research on wind turbine rotor models using NACA profiles. Renewable Energy 33, 1721–1732.
Wang, F., Bai, L., Fletcher, J., Whiteford, J., Cullen, D., 2008. The methodology for aerodynamic study on a small domestic wind turbine with scoop. Journal of Wind Engineering and Industrial Aerodynamics 96, 1–24.
Yurdusev, M.A., Ata, R., Çetin, N.S., 2006. Assessment of optimum tip speed ratio in wind turbines using artificial neural networks. Energy 31, 2153–2161.